3B2v7.51c GML4.3.1 Emsat : 100146 Prod.Type: pp.1−11(col.fig.:NIL) ED:Mahashankar PAGN: ashok SCAN: Naresh

Magnetic Microwires: Manufacture, Properties and Applications

Amorphous metallic materials take a prominent position among metallic materials due to their unique and favorable association of physical properties related to the absence of long-range order. These materials possess superior mechanical, electrical, magnetic, and chemical properties (see *Metallic glasses*; *Amorphous Intermetallic Alloys: Resistivity; Amorphous and Nanocrystalline Materials*). The use of preparation methods that allow rapid condensation of atoms or rapid solidification of liquid metallic melts in order to avoid cryztallisation is necessary to achieve the energetically metastable amorphous state. The formation of the amorphous state depends on the alloy composition as well on the process conditions. Presently known amorphous metallic materials have been obtained in shapes like thin films (Chan <Bib7>1993), ribbons (Boll <Bib6>1983), wires (Hagiwara and Inoue <Bib12>1993), powders (Yagi *et al.* <Bib34>2000), and very recently bulk materials with dimensions in the range of millimeters (Inoue <Bib14>2000). Amorphous metallic materials are used in applications based on their outstanding properties, but the most important are those based on magnetic properties, their soft magnetic behavior leading to high permeability and low coercivity.

Amorphous ribbons have been used in transformer cores, magnetic recording heads, and in sensing elements. The amorphous metallic wires have attracted much interest due to their more convenient shape, dimensions, and specific properties emerging from their degree of symmetry. Amorphous metallic wires with diameters ranging between 80 μm and 160 μm are obtained by the so-called in-rotating water quenching, technique (Ogasawara <Bib21>1995). This procedure implies a very high cooling rate from the molten alloy and gives rise to local magnetoelastic anisotropies from the coupling between internal stresses and magnetostriction. These internal stresses originate from the thermal gradient present during the quenching, and their order of magnitude, around 10^2 MPa, is determined by Young's modulus, the Poisson coefficient, and the average temperature during fabrication.

The main interest of amorphous wires is related with the cylindrical geometry and magnetostriction constant. In the latter case, in Fe-rich alloys, the magnetization process is characterized by a single Barkhausen jump (Vázquez and Chen <Bib29>1995) associated with a square hysteresis loop. This behaviour, that it is observed above a critical length of 7 cm, is determined by a particular domain structure originating from stresses induced in the wire during the fabrication procedure. Current and voltage transformers and magnetic sensors have been developed based on this effect (Mohri *et al.* <Bib20>1984). On the other hand, Co-rich alloys exhibit vanishing magnetostriction and do not show bistability (Gómez-Polo and Vázquez <Bib11>1993). Although the saturation magnetization is low, the outstanding properties of this material are related with a high initial susceptibility and with another effect, strongly connected with the geometrical shape, known as magnetoimpedance effect. The latter induces wire impedance variations by magnetic field application (Beach and Berkowitz <Bib5>1994, Panina and Mohri <Bib22>1994). This effect can be used in magnetic sensors for detecting magnetic fields.

In contrast, glass-coated microwires are obtained by an extracting melt-spinning technique, based on Taylor's classical method (Taylor <Bib26>1924). The tiny dimensions and the outstanding magnetic behaviors at low-, medium- and high-frequency magnetic fields make them very useful for practical purposes.

1. *Material Preparation: Production Technique of Amorphous Glass-covered Metallic Microwires*

The production of glass-covered metallic microwires is presently achieved by the glass-coated extracting melt-spinning method. The basic idea of this method was initially proposed by Taylor <Bib26>(1924) and improved by Ulitovsky <Bib28>(1932) and Parkhachev <Bib23>(1966). Figure 1 shows a schematic diagram of the method. It consists in the rapid drawing of a softened glass capillary in which the molten metal is entrapped. The capillary is drawn from the end of a glass tube containing the molten alloy. Previously, a metallic pellet of the master alloy, prepared by induction melting of pure elements, has been placed inside the sealed end glass tube and then the alloy is melted by a high-frequency field of an inductive coil and the end of the glass tube is softened. Hence, around the molten metal drop, there is a softened glass cover which allows the drawing of the capillary. A low level of vacuum (~50–200 Pa of an inert gas atmosphere) within the glass tube prevents metal oxidation. It also assures stable melt-drawing conditions, in conjunction with induction heating, employing the levitation principle. In order to ensure continuity of the process, there is a glass tube displacement with a uniform feed-in speed between 0.5 mm $min^{-1}$and 10 mm min^{-1}. The rapid cooling rate required to obtain an amorphous structure, between 10^5 K s^{-1} and 10^6 K s^{-1}, is reached by cooling the as-formed wire by a water jet at approximately 1 cm under the high-frequency induction coil.

It is clear both intuitively and from the available literature (Donald <Bib10>1987) that the successful production of high-quality, continuous filaments of

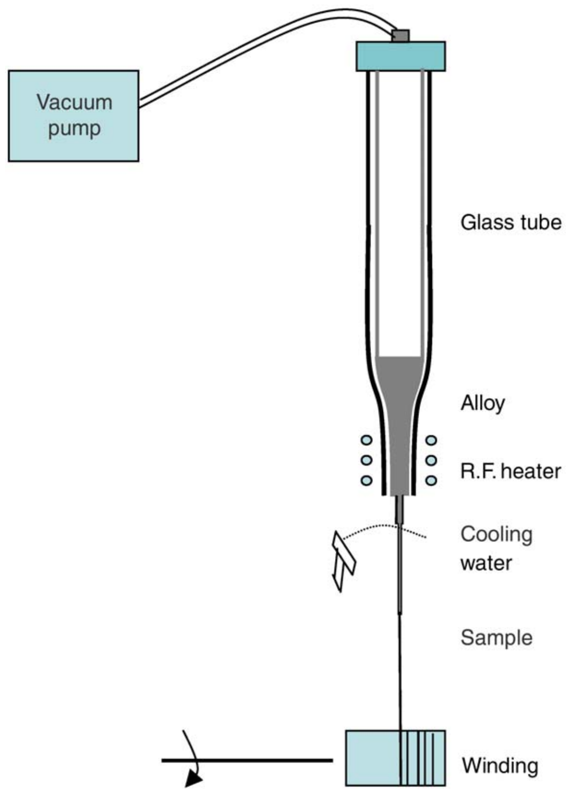

Figure 1
Schematic diagram of the glass-coated melt spinning
AQ8 method.

given dimensions by the Taylor-wire technique is dependent on a number of critical materials and process factors. These are summarized below.

The materials selection is crucial in order to be successful. In the case of amorphous metallic alloys the composition chosen should be that of a glass former. It is well known (Chiriac and Ovary < Bib9 >1997) that glass formation is favored at compositions for which the liquid is relatively stable compared to crystalline phases. This relative stability also correlates with the sizes of the atomic species in the alloy (see *Metallic Glasses*).

Once the alloy composition is chosen, the glass should be well selected in order to allow a properly glass-coated fabrication. It must be compatible with the metal or alloy at the drawing temperature to avoid, as much as possible, chemical reaction between glass and metal. Its working (drawing) temperature must be higher than the melting point of the metal or alloy employed, but below its boiling point and below the temperature at which the metal vapor pressure becomes high enough to disrupt the process. The viscosity–temperature behavior of the glass must allow easy fiber drawing in the temperature range of interest and its crystallization temperature should be higher than the working temperature.

The thermal expansion coefficient of the glass should be matched to, or be slightly less than, that of the metal or alloy of interest. The viscosity of the glass coating must attain a high enough value, where further extension during drawing cannot occur before the metal core has solidified. Otherwise, if the core is solid and the coating continues to extend, metal core fracture will be initiated and a discontinuous product will be obtained.

In practice, because glass is used in the form of tubes of uniform dimensions in the Taylor-wire process, the choice of specific glass compositions is severely restricted due to the limited range of commercial offers. This restricts the choice to Pyrex-type borosilicate compositions or to fused silica.

As it will be reported later, two main factors are predominantly responsible for the microwire magnetic behavior, i.e., the metallic core microstructure and the ratio of the metallic core radius to the total radius of the microwire $\rho = R_m/R$ (Chiriac and Óvári
< Bib9 >1997). These microstructural and geometri- QA:1
cal factors can be controlled by process conditions. A good control of melting temperature allows the obtention of amorphous and partially nanocrystallized samples. The most important factor governing the core diameter of the filament seems to be the take-up speed; the higher the speed, the smaller the fiber dimensions obtained. Another important factor is the vacuum level. In practice, the metal thickness is indirectly controlled by a measurement device based on emission and reception antennas that acts on the vacuum pump when the metal diameter deviations are detected. The thickness of glass coating depends mainly on the feed-in rate of the glass tube, but also depends, to a lesser degree, on the thickness of the glass tube employed, and the take-up speed.

Figure 2 shows a photograph corresponding to a microwire scanning electron microscope (SEM) image. The composition is $(Fe_{30}Co_{70})_{72.5}Si_{12.5}B_{15}$ and corresponding dimensions are a total diameter D of 12 μm and a metal nuclei diameter D_m of 3.5 μm.

2. *Magnetic Properties*

A large variety of magnetic alloys (Hernando and Vázquez < Bib13 >1993) can be fabricated mainly based on iron and cobalt. The high mechanical strength and the ferromagnetic character make them attractive as reduced size components in electronics, for magnetic recording, biomedical implantations, etc. Their high-frequency behavior can also be exploited in devices for electromagnetic power absorption.

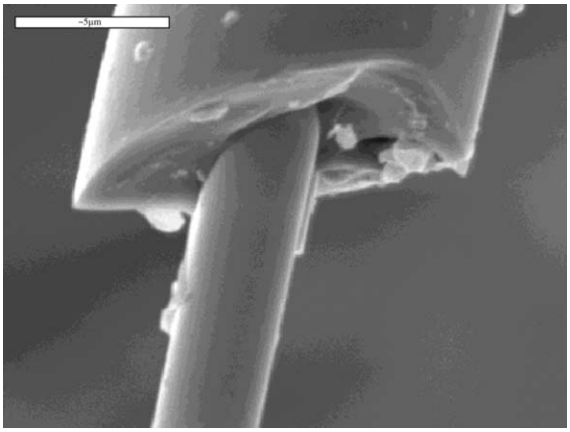

Figure 2
SEM photograph of an $(Fe_{30}Co_{70})_{72.5}Si_{12.5}B_{15}$ amorphous magnetic microwire with total diameter $D =$ 12 μm and metal core diameter $D_m = 12$ μm (Photograph: courtesy of H. García-Miquel, UPV Valencia, SPAIN).

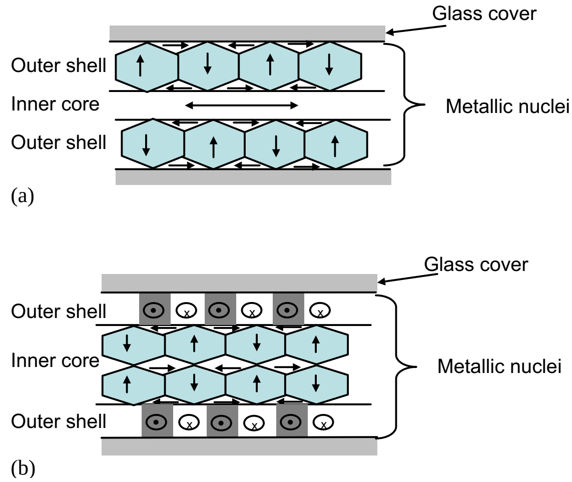

Figure 3
Schematic diagram of the estimated domain structure in positive (a) and negative (b) magnetostrictive amorphous glass-coated microwires (Chiriac *et al.* <Bib9>1997).

2.1 Magnetic Domains and Low-frequency Axial Hysteresis Loop

The hysteresis loop shape is strongly dependent on the composition of the metallic core. The magnetization process is strongly dependent on the magnetostriction constant and the magnetoelastic anisotropy induced by internal stresses (Vázquez *et al.*
QA:2 <Bib30>1996). Glass coating induces an extra radial internal stress due to the different thermal expansion coefficients of the nucleus and the glass. Besides, the extraction tensile stress induces an axial internal anisotropy. The coupling determines the domain structure, an inner axial single domain, and the outer shell.

As shown in Fig. 3, in positive magnetostrictive microwires (Fe-rich), the inner core has an easy magnetization direction along the axis and the outer-shell easy direction is perpendicular to the axis. In negative magnetostrictive microwires (Co-rich), the inner-core easy magnetization is perpendicular to the axis direction while the external shell adopts circular directions. Magnetic microwire behavior is determined by this type of domain structure.

Positive magnetostrictive microwires show a square hysteresis loop with large Barkhausen jump. This effect results from the magnetization reversal in the inner core at a given value of the axial magnetic field, called switching field, H^*. The value of the switching field depends on the average value of the uniaxial anisotropy constant of the inner core, and consequently on the level of the internal stresses. These thermoelastic internal stresses depend on the mechanical, thermal properties and the cross-sectional ratio of glass and metal (Baranov
<Bib4>2001), $x = (R/R_m)^2 - 1 = (1/\rho^2) - 1$. QA:3

The general equation describing the internal stresses can be simplified, considering $n_1 = n_2 = \frac{1}{3}$ where n_i are the Poisson coefficients of crystal and metal, respectively. They can be expressed as follows in a cylindrical coordinate system:

$$\sigma_z = \sigma_0 \frac{kx}{kx+1}\frac{(k+1)x+1}{(k/3+1)x+4/3} \tag{1}$$

$$\sigma_r = \sigma_\phi = \sigma_0 \frac{kx}{(k/3+1)x+4/3} \tag{2}$$

where $\sigma_0 = E_1(a_1 - a_2)(T^* - T)$, k is the ratio of the Young's moduli $k = E_2/E_1 = 0.3{-}0.6$.

The internal stresses cause the appearance of magnetoelastic anisotropy, corresponding to a magnetic field:

$$H_a = \frac{\lambda\sigma_0}{M}\frac{Kx}{Kx+1}F(k,x) \tag{3}$$

were $F(k,x)$ is a slowly varying function of k and x.

Figure 4 shows the composition dependence of microwire hysteresis loops. Figures 4(a) and 4(b) are for microwires of the compositions $Fe_{70}Si_{10}B_{15}C_5$ and $Co_{60}Fe_{15}Si_{15}B_{10}$, respectively. Magnetic bistability is clearly observed in both cases. In turn, Fig. 4(c) shows a nonbistable loop for a $Co_{68.5}Si_{14.5}B_{14.5}Y_{2.5}$ alloy microwire. The main difference derived from the various compositions of the three microwires is the magnetostriction constant, λ_s. The corresponding

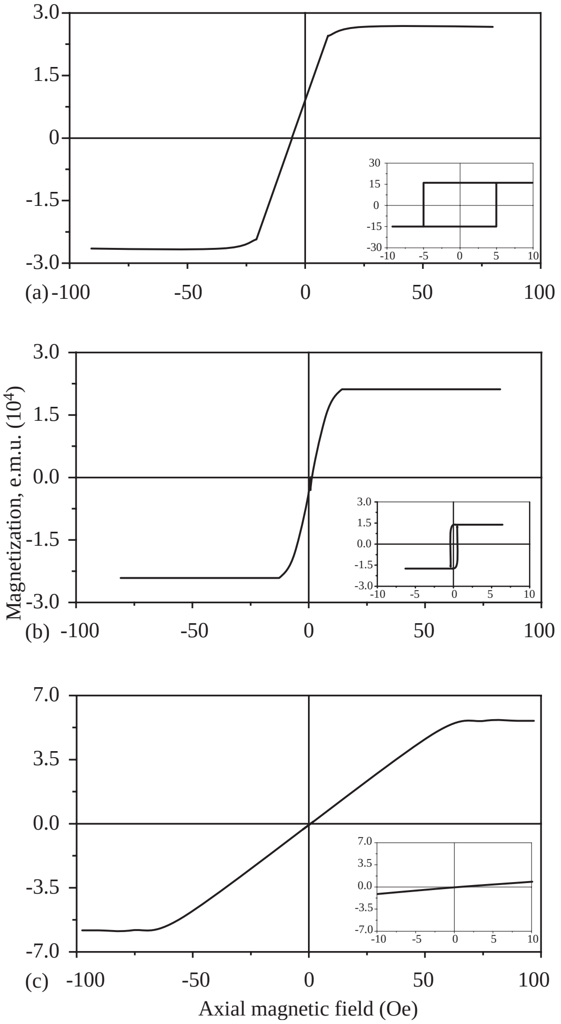

Figure 4
AQ9 Low-field (inset) and high-field hysteresis loops for
AQ10 microwires of $Fe_{70}Si_{10}B_{15}C_5$ (a), $Co_{60}Fe_{15}Si_{15}B_{10}$ (b), and $Co_{68.5}Si_{14.5}B_{14.5}Y_{2.5}$ (c) alloys.

values for Figs. 4(a)–(c) are 2×10^{-5}, 1×10^{-7}, and -2×10^{-6}, respectively. Accordingly, microwires with large and positive λ_s show magnetic bistability, whereas those having intermediate negative λ_s do not show that behavior. The microwire with nearly zero but positive λ_s (Fig. 4(b)) also shows bistable behaviour. In fact, as reported by Baranov *et al.* <Bib3>(1995), the bistability disappears when λ_s changes its sign from positive to negative.

On the other hand, the ratio $\rho = R_m/R$ between the radius of the metallic core, R_m, and the total radius, R, of the microwire plays an important role in determining the parameters of the hysteresis loop.

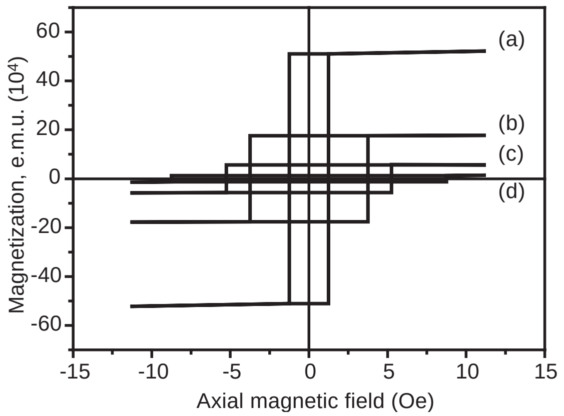

Figure 5
Hysteresis loops for $Fe_{89}Si_3B_1C_3Mn_4$ microwires with different ratio $\rho = R_m/R$ between the radius of the metallic core, R_m, and the radius of the microwire, R, for $\rho = 0.2$ (a), $\rho = 0.25$ (b), $\rho = 0.28$ (c), and $\rho = 0.6$ (d).

Figure 5 shows the bistable loops as a function of ρ. A higher longitudinal anisotropy due to thinner inner core is associated with a higher anisotropy field, H_k, and lower remanence.

The hysteresis loop behavior can be tailored by means of annealing. Amorphous structural relaxation and nanocrystallization (Vázquez *et al.* <Bib33>1999, Marín *et al.* <Bib18>1997) can change the microwire anisotropy field leading to a broad spectrum of magnetic behaviors with different hysteresis loops which is very interesting from the applications point of view.

2.2 *High Magneto-impedance Effect*

The magneto-impedance effect has been recently discovered in soft amorphous wires with very high circular permeability (Beach and Berkowitz <Bib5>1994, Panina and Mohri <Bib22>1994). It consists of a large relative change (up to around 400%) of the impedance (both real and imaginary parts) upon application of a d.c. magnetic field or stress. In order to measure the impedance, typically a low-density current flows along the sample having a frequency in the range of MHz. This effect has been detected in nearly zero magnetostriction Co-base samples of the shape of a wire, ribbon, or thin film. It has been interpreted as arising from the classical skin effect, the penetration depth of which is defined as

$$\delta = (\rho/\pi\mu f)^{1/2} \tag{4}$$

ρ being the electrical resistivity, f the frequency, and μ the transverse permeability.

Upon application of a d.c. field, the permeability decreases, and accordingly δ increases until it reaches the radius of the wire which finally results in an effective change of the impedance, Z, considered for a magnetic conductor given by

$$Z = R_{\mathrm{dc}}(kR)J_0(kR)/2J_1(kR) \tag{5}$$

with $k = (1+j)/\delta$ where J_0 and J_1 are the Bessel functions and R the radius of the microwire (Chen *et al.* < Bib8 >1998).

Amorphous microwires show also magneto-impedance effects and they are found to be more promising for several applications compared to wires and ribbons because of their tiny dimensions and protective glass coating. The influence of domain structure on this effect has been observed for vanishing negative (Vázquez *et al.* < Bib32 >1998) and positive (Mandal *et al.* < Bib17 >2000) magnetostrictive microwires.

Figure 6 (Vázquez *et al.* < Bib32 >1998) shows the magneto-impedance effect for $Co_{68.5}Mn_{6.5}Si_{10}B_{15}$ microwires with a metallic diameter of about 14 µm and an insulating glass coating thickness of 5 µm. The wire displays a nonbistable hysteresis loop similar to that shown in Fig. 4(c) associated with a very low and negative magnetostriction constant ($\lambda_s \sim 10^{-7}$). The negative nature of λ_s is deduced from the increase of the anisotropy field upon application of a tensile stress. A bamboo-like domain structure can be

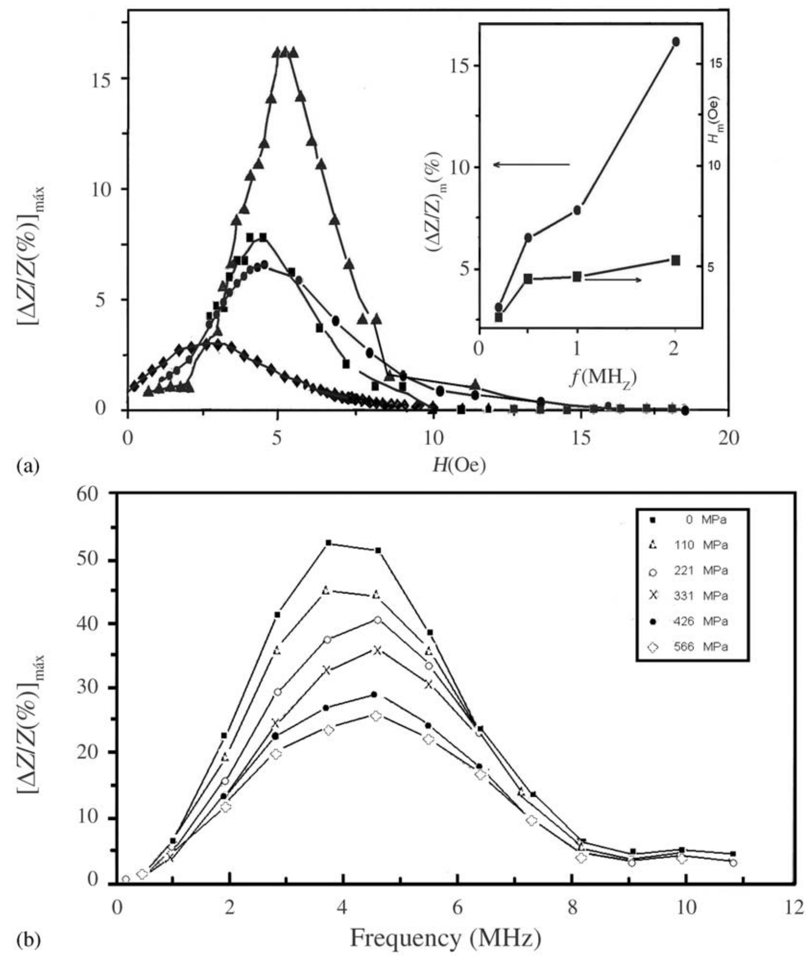

Figure 6
(a) Magneto-impedance effect of an as-prepared $Co_{68}Mn_7Si_{10}B_{15}$ sample at different frequencies (I = 2.9 mA) of a.c. current: 0.2 MHz (♦), 0.5 MHz (•), 1 MHz (■), 2 MHz (▲). The inset shows the dependences $(\Delta Z/Z)_m$ and H_m on frequency of a.c. current, (Vázquez *et al.* 1998). (b) The variation of maximum percentage change in magneto-impedance (i.e., the peak value of giant magneto-impedance), $(\Delta Z/Z)_m$ with frequency under different axial tensile stresses with 1 mA a.c. current through the sample. Mandal *et al.* 2000).

assumed, as in the case of negative magnetostriction amorphous wires obtained by the in-rotating-water quenching technique (Yamasaki <Bib35>1992).

The existence of $(\Delta Z/Z)_{\mathrm{m}}$ for a given H_{m} has been reported for samples heated in the presence of a transverse magnetic field (Sommer and Chien <Bib24>1996) or tensile stress (Tejedor *et al.* <Bib25>1996) where a circular magnetic anisotropy is deliberately induced. In the present case such anisotropy spontaneously appears from the coupling between internal stress and magnetostriction. Then it seems likely that the appearance of $(\Delta Z/Z)_{\mathrm{m}}$ is associated with the existence of a transverse circular anisotropy. In fact, the maxima in Fig. 6 should be ascribed to the maximum value of the circular permeability, where according to Eqn. (4) the penetration depth reaches a minimum.

The effect of applying an increasing axial field, H, is to balance the anisotropy field H_{k}. Consequently, $(\Delta Z/Z)_{\mathrm{m}}$ is observed for $H = H_{\mathrm{k}}$. Further increase of H gives rise to reduction of the circular permeability and to a final decrease of impedance. The increase of $(\Delta Z/Z)_{\mathrm{m}}$ with frequency (see inset of Fig. 6(a)) should be, in principle, ascribed to a stronger skin effect (Eqn. (4)).

The magneto-impedance effect has also been observed for very low and positive magnetostriction in a $Co_{83.2}Mn_{7.6}Si_{5.8}B_{3.3}$ microwire having a hysteresis loop similar to Fig. 4(b). As shown in Fig. 6(b) (Vázquez *et al.* <Bib32>1998) a change of more than 50% in magneto-impedance has been observed for this sample. It has been obtained for a 140 Oe d.c. magnetic field along the length of the microwire. The application of external stress can change the magneto-impedance magnitude to a large extent, which opens the possible application of microwires as stress sensors.

In this case, the giant magneto-impedance can be explained by considering the change in penetration depth, δ, due to the change in circular permeability according to Eqn. (4) caused by the application of a magnetic field. The applied d.c. magnetic field nearly compensates the axial magnetic anisotropy when it reaches the switching field of the sample. At this field, the quasi-free magnetization responds quickly to the external oscillating magnetic field and gives rise to a large circular permeability. As the switching field of our low-magnetostrictive sample is very small, a few mOe, the maximum value of the giant magneto-impedance is observed close to $H_{\mathrm{dc}} = 0$. When the external d.c. field is increased beyond the switching field, the circular permeability decreases owing to the unidirectional magnetostatic anisotropy caused by H_{dc}. Therefore, with the increase of a d.c. magnetic field, the increase in penetration depth, δ, results in a decrease in magneto-impedance.

The applied tensile stress generates a uniaxial anisotropy along the axis of the wire and increases the volume of the inner-core domain. As a result of it, the circular permeability and hence the value of magneto-impedance becomes reduced with the increase of stress (Fig. 6(b)).

2.3 Ferromagnetic and Natural Ferromagnetic Resonance

Technologically, the study of microwave properties is also very promising. In the microwave region (approaching GHz range), ferromagnetic resonance occurs, which is accompanied by absorption of energy at the resonance frequency.

Using the equation of Kittel for a plane (Kittel <Bib15>1948), the resonance frequency f_{r} can be calculated by means of

$$f_{\mathrm{r}} = \frac{g}{2\pi}\sqrt{(H_{\mathrm{a}} + 4\pi M)(H_{\mathrm{a}} + H)} \tag{6}$$

Here H_{a} is the anisotropy field, M the magnetization, g the gyromagnetic ratio, and H the external applied magnetic field. At that frequency, the permeability increases dramatically and the skin depth is very small (less than 1 μm). Ferromagnetic resonance (FMR) is connected with spin precession about the magnetization vector due to the effect of a high-frequency electromagnetic field applied such that the magnetic component is perpendicular to the magnetization vector (Antonenko *et al.* <Bib1>1997). As a rule, the observation of FMR needs the application of an external d.c. magnetic field which provides a uniform magnetization of the examined sample.

One of the most interesting phenomena observed in amorphous ferromagnetic cast microwire is natural ferromagnetic resonance (NFMR) (Kraus *et al.* <Bib16>1981, Baranov <Bib2>1988). The NFMR was observed in ferrite without the application of an external magnetic field. The cause of NFMR is the internal magnetic anisotropy. The frequency depends on the value of the magnetic anisotropy. In known materials, the NFMR frequency is less than 1 GHz.

The appearance of NFMR, in positive magnetostrictive microwires, characterized by a single well-distinguished line in the range 2–10 GHz indicates the existence of a large magnetic anisotropy. Generally, the magnetic component of the a.c. field is perpendicular to the microwire axis, so the internal magnetic anisotropy causes the microwire to be magnetized along its axis. This conclusion agrees with the axial magnetization presented by positive magnetostrictive microwires associated with bistable magnetic behavior.

Due to the high resonance frequency (up to 10 GHz) and the extremely large magnitude of the permeability ($\mu'' > 100$), microwires are of great importance for utilization as radio-frequency absorbing materials. The NFMR in the range from 2 GHz to 10 GHz is observed in all amorphous microwires with positive magnetostriction constant.

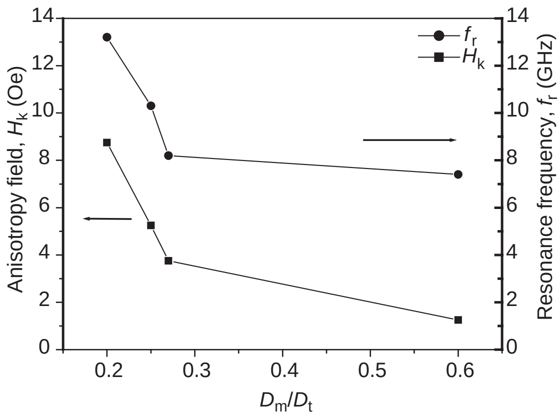

Figure 7
Dependence of anisotropy field, H_k, and natural ferromagnetic resonance on the ratio $\rho = R_m/R = D_m/D_t$ of $Fe_{89}Si_3B_1C_3Mn_4$ microwires shown in Fig. 5.

The NFMR frequency can be calculated by taking into account that the depth of the skin layer, δ, is smaller than the radius of the microwire, r. Using Kittel's equation (Eqn. (6)) for plane and considering $H = 0$, one finds

$$f_r = \frac{g}{2\pi}\sqrt{(H_a + 4\pi M)H_a} \tag{7}$$

If $H_a \ll 4\pi M$, Eqn. (5) can be written as

$$f_r = \left(\frac{g^2 M H_a}{\pi}\right)^{1/2} \tag{8}$$

Considering H_a as given by Eqn. (3) the resonance frequency can be given as

$$f_r = \left(\frac{\lambda\sigma_0 g^2}{\pi}\frac{kx}{kx+1}F(k,x)\right)^{1/2} \tag{9}$$

Equation (8) shows that there is a strong dependence of the resonance frequency on composition, through the magnetostriction constant, and on fabrication conditions, through x and σ_0. Figure 7 illustrates the dependence of the anisotropy field, H_k, and the natural ferromagnetic resonance frequency on the ratio $\rho = R_m/R$ for the $Fe_{89}Si_3B_1C_3Mn_4$ microwires shown in Fig. 5.

3. *Applications*

A broad number of applications can be developed using amorphous magnetic microwires (Marín *et al.* < Bib18 >1997) that are based on the magnetic properties discussed above. Magnetic tags and magnetic detectors based on the bistable magnetic behavior or on the high magnetic susceptibility can be developed to work at low frequencies. Stress, current, position, liquid level or pressure sensors, and magnetic field detectors are based on giant magneto-impedance effect and would work at medium frequency. This type is employed in technologies such as car traffic monitoring, quality control of steels, vibrational detection of earthquakes, or biomagnetic sensors. Ferromagnetic resonance can be used to develop tags for article electronic surveillance and for electromagnetic wave shielding. In the following sections two particular applications are described.

3.1 *Magnetic Tag*

One of the applications consists in the use of several Fe-based magnetostrictive microwires for sensing elements in magnetic tags. The tag contains several microwires with well-differentiated coercivity, all of them characterized by a bistable magnetic loop. Once the magnetic tag is submitted to an increasing magnetic field, each particular microwire reverses its magnetization resulting in an electrical signal on a coil system (Vázquez and Zhukov < Bib31 >1996).

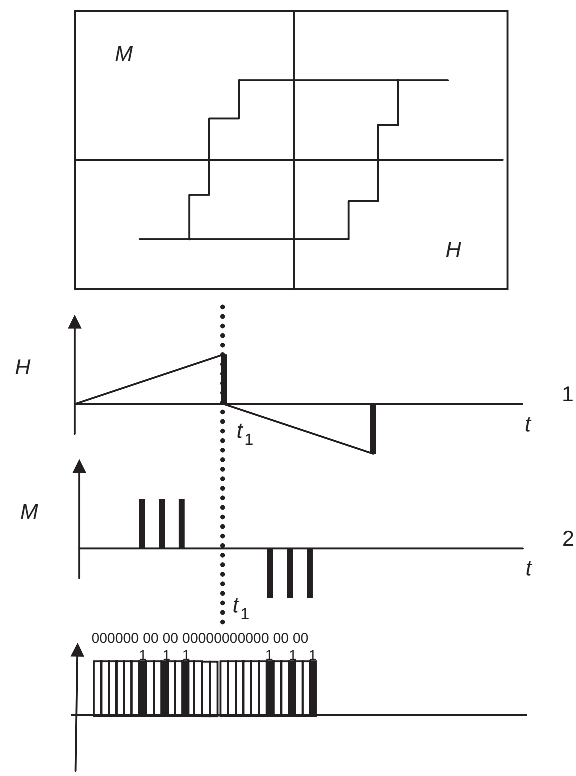

Figure 8
Schematic representation of the working system of a magnetic tag as described in the text (Vázquez *et al.* ES Patent 9601993).

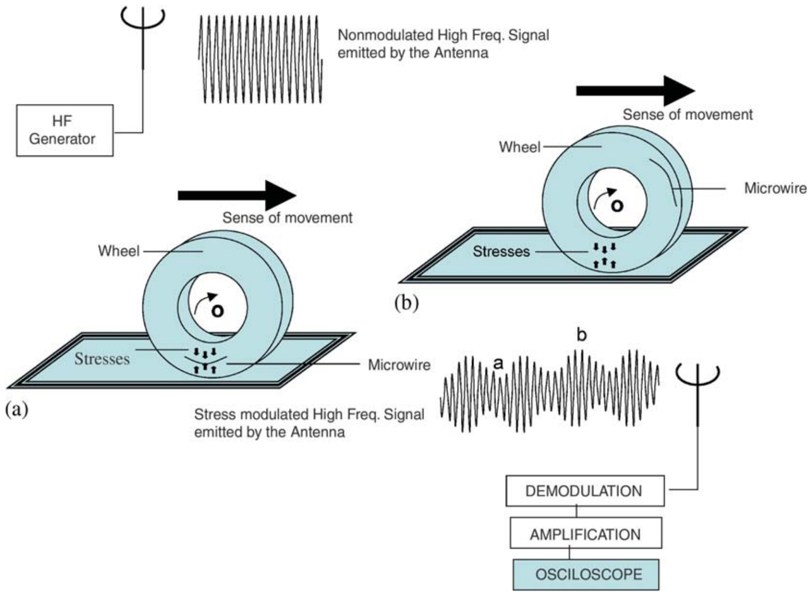

Figure 9
Schematic representation of a wireless stress sensors for vehicle tires.

Figure 8 shows the schematic representation for a working system of a magnetic tag as described here.

3.2 Wireless Stress Sensor for Vehicle Tires

This application is based on the stress dependence of the magneto-impedance effect. The sensor system monitors the frictional conditions between the tire and the roadway in order to enhance vehicle safety.

It has been shown that the stress measured at suitable positions in a car tire can be analyzed to give information on the frictional coefficient, the roadway conditions, and the tire inflaction. The sensor proposed here (Tyren *et al.* < Bib27 >2000) is based on a combination of magnetostriction and magneto-impedance. The stress produces a change in the permeability in the magnetoelastic microwire. Thus, the skin depth of this element is altered leading to a change in its electrical impedance. This results in amplitude variations measured by a radio-frequency link between the sensor and stationary antenna. Figure 9 shows a scheme of the basic principles of the sensor.

See also: Metallic Filaments; Magneto-impedance Effects in Metallic Multilayers 100127; Magnetoelasticity in Nanoscale Heterogeneous Materials 100136.

Bibliography

< Bib1 >Antonenko A N, Baranov S A, Larin V S, Torkunov A V 1997 Natural ferromagnetic resonance in cast microwires covered by glass insulation. *J. Mater. Sci. Eng* **A248**, 248–50

< Bib2 >Baranov S A 1988 Magnetic properties of amorphous microwire in the microwave range. *Zh. Teor. Fiz* **68** (1), 136–7

< Bib3 >Baranov A S, Larin V S, Torkunov A V, Zhukov A P, Vázquez M 1995 Magnetic properties of glass insulated amorphous microwires. In: Vázquez M, Hernando A (eds.) *Nanocrystalline and Non-crystalline Materials*. World Scientific, Singapore, pp. 567–71

< Bib4 >Baranov S A 2001 Evaluation of the distribution of residual stresses in the cord of amorphous microwire. *Metal Sci. and Heat Treat* **43** (3–4), 167–8

< Bib5 >Beach R S, Berkowitz A E 1994 Giant magnetic field dependent impedance of amorphous FeCoSiB wire. *Appl. Phys. Lett* **64**, 3652–4

< Bib6 >Boll R, Hilizinger H R, Warlimont H 1983 Magnetic material properties and applications of metallic glasses. In: Hasegawa R (ed.) *The Magnetic, Chemical and Structural Properties of Glassy Metallic Alloys*. CRC Press, Boca Raton, FL, pp. 183–201

< Bib7 >Chan R W 1993 Background to rapid solidification processing. In: Liebermann H H (ed.), *Rapidly Solidified Alloys*. Dekker, pp. 1–15 QA:4

< Bib8 >Chen D X, Muñoz J L, Hernando A, Vázquez M 1998 Magnetoimpedance of metallic ferromagnetic wires. *Phys. Rev. B* **57** (17), 10699–704

< Bib9 >Chiriac H, Óvári T A 1997 Amorphous glass-covered magnetic wires: preparation, properties, applications. In: *Progress in Materials Science*. Vol. 40. Elsevier, Great Britain, pp. 333–407

< Bib10 >Donald I W 1987 Production, properties and applications of microwire and related products. *J. Mater. Sci.* **22**, 2661–79

< Bib11 >Gómez-Polo C, Vázquez M 1993 Structural relaxation and magnetic properties of Co-rich amorphous wire. *J Magn. Magn. Mater* **118**, 86–92

< Bib12 >Hagiwara M, Inoue A 1993 Production techniques of alloy wires by rapid solidification. In: Liebermann H H (ed.) *Rapidly Solidified Alloys*. Dekker, New York, pp. 141

< Bib13 >Hernando A, Vázquez M 1993 Engineering properties of rapidly solidified alloys. In: Liebermann H H, (ed.), QA:5 *Rapidly Solidified Alloys*, pp. 553–89

< Bib14 >Inoue A 2000 Stabilization of metallic supercooled liquid and bulk amorphous alloys. *Acta Mater* **48**, 279–306

< Bib15 >Kittel C 1948 On the theory of ferromagnetic resonant absorption. *Phys. Rev* **73**, 155–61

< Bib16 >Kraus L, Frait Z, Schneider I 1981 Ferromagnetic resonance in amorphous $(FeNi)_{80}P_{10}B_{10}$ alloys. *Phys. Status. Solidi. (a)* **63**, 669–75

< Bib17 >Mandal K, Puerta S, Vázquez M, Hernando A 2000 Giant magnetoimpedance in amorphous $Co_{83.2}Mn_{7.6}$-$Si_{5.8}B_{3.3}$. *Phys. Rev. B* **62** (10), 6598–602

< Bib18 >Marín P, Arcas J, Zhukov A, Vázquez M, Hernando A 1997 Evolution of magnetic properties with annealing temperature for CoMnSiB microwires. In: Hadjipanayis G C (ed.) *Magnetic Hysteresis in Novel Magnetic Materials*. Kluwer Academic, The Netherlands, pp. 743–8

< Bib19 >Marín P, Hernando A 2000 Application of amorphous and nanocrystalline magnetic materials. *J. Magn.* QA:6 *Magn. Mater* **215–216,** 729–34

< Bib20 >Mohri K, Humphrey F B, Yamasaki J, Okamura K 1984 Jitter-less pulse generador elements using amorphous biestable wire. *IEEE Trans. Magn* **MAG-20**, 1409–11

< Bib21 >Ogasawara I, Ueno S. 1995 Preparation and proper- QA:7 ties of amorphous wires. *IEEE Trans. Magn.* **31,** 1219–123

< Bib22 >Panina L, Mohri K 1994 Magnetic-impedance effect in amorphous wires. *Appl. Phys. Lett* **65**, 1189–91

< Bib23 >Parkhachev,V N, 1966 Installation for production of glass insulated microwire directly from liquid metal. *US Patent* 3,256,584

< Bib24 >Sommer R L, Chien C L 1996 Giant magnetoimpedance effects in metglas 2705M. *J. Appl. Phys* **79** (8), 5140–3

< Bib25 >Tejedor M, Hernando B, Sánchez M L, García-Arribas A 1996 Influence of induced anisotropy on magneto-impedance in Co-rich metallic glasses. *J. Magn. Magn. Mater* **157/158**, 141–2

< Bib26 >Taylor G F 1924 A method for drawing metallic filaments and discussion of their properties and uses. *Phys. Rev* **24**, 6555–60

< Bib27 >Tyren C, Vázquez M, Hernando A, Quiñónez C 2000 Stress-wire sensor. *Patent* WO00/57147

< Bib28 >Ulitovsky A, 1932 Electrical adjustable resistance. *US Patent* 369,646

< Bib29 >Vázquez M, Chen D X 1995 The magnetization reversal in amorphous wires. *IEEE Trans. Magn* **31**, 1229–38

< Bib30 >Vázquez M, Zhukov A P, Antonenko A, Larin V, Torkunov A 1996 Método de codificación y marcado magnético de objetos. *ES Patent* P9601993

< Bib31 >Vázquez M, Zhukov A P 1996 Magnetic properties of glass-coated amorphous and nanocrystalline wires. *J. Magn. Magn. Mater* **160**, 223–8

< Bib32 >Vázquez M, Zhukov A P, Aragoneses P, Arcas J, García-Beneytez J M, Marín P, Hernando A 1998 Magneto-impedance in glass-coated amorphous microwires. *IEEE Trans. Magn* **34**, 724–8

< Bib33 >Vázquez M, Marín P, Arcas J, Hernando A, Zhukov A P, González J 1999 Influence of nanocrystalline structure on the magnetic properties of wires and microwires. *Textur. Microstruc* **32**, 245–67

< Bib34 >Yagi M, Endo I, Otsuka I, Yamamoto H, Okuno R, Koshimoto H, Shintani A 2000 Magnetic properties of Fe-based amorphous powder cores produced by a hot-pressing method. *J. Magn. Magn. Mater* **215–216**, 284–7

< Bib35 >Yamasaki J 1992 Sensing function and amorphous magnetic materials. *J. Magn. Soc. Japan* **16**, 14–26

P. Marín and A. Hernando

Encyclopedia of Materials: Science and Technology
ISBN: 0-08-043152-6
pp. 1–9

Title: Encyclopedia of Materials: Science and Technology (EMSAT)
Article/Number: Magnetic Microwires: Manufacture, Properties and Applications/100146

Dear Author,
During the preparation of your manuscript for typesetting some questions have arisen. These are listed below. Please check your typeset proof carefully and mark any corrections in the margin of the proof or compile them as a separate list. This form should then be returned with your marked proof/list of corrections to Elsevier Science.

Information in margins: "SX000" codes relates to the subject index and "6-digit numbers" refer to cross-references to other articles in EMSAT.

This form should then be returned with your marked proof/list of corrections to Aimee Bishop (a.bishop@elsevier.co.uk; fax no. +44 (0) 1865 843974) at Elsevier Science, Major Reference Works, The Boulevard, Langford Lane, Kidlington, Oxford OX5 1GB.

Queries and/or remarks

QA:8	Make sure permission to use figures 3 & 6 has been granted
QA:1	Check the change from ''Chirac 1997'' to 'Chirac and Ovari 1997'. OK?
QA:2	Check the change from 'Vazquez 1996' to 'Vazquez et al. 1996'. OK?
QA:3	Check the deletion of OK?
QA:4	Place of publication?
QA:5	Pls provide publisher & place
QA:6	Check the deletion of 'Hernado'. OK?
QA:7	Check the page range
QA:9	In fig. 4, please check the change along the y-axes.
QA:10	In fig.4, please check the continuity of the line which is encircled in 4(b) and 4(c).